Relativistic convergent close-coupling method: Calculations of electron scattering from cesium

Dmitry V. Fursa,* Christopher J. Bostock, and Igor Bray
ARC Centre for Antimatter-Matter Studies, Curtin University, Perth 6845, Australia
(Received 11 May 2009; published 28 August 2009)

We present a detailed formulation of the relativistic convergent close-coupling (RCCC) method which is based on the solution of the Dirac equation describing electron scattering from quasi-one-electron atoms. A square-integrable Dirac *L* spinor basis has been used to obtain a set of target states representing both the bound and continuum spectra of the target. A set of momentum-space coupled Lippmann-Schwinger equations for the *T* matrix is then formulated and solved. We use spin asymmetries, particularly those that are identically zero in a nonrelativistic formulation, to check the accuracy of the RCCC method and find good agreement with experiment on a broad energy range.

DOI: 10.1103/PhysRevA.80.022717 PACS number(s): 34.80.Bm, 34.80.Dp, 34.80.Nz

I. INTRODUCTION

We have recently reported the development of the relativistic convergent close-coupling (RCCC) method and illustrated it by application to the elastic electron scattering from cesium atoms at a single incident electron energy of 7 eV [1] and also to the study of electron scattering from gold atoms [2]. The aim of this paper is to provide details of the method and demonstrate its ability to produce accurate collision results across a wide energy range.

The nonrelativistic formulation of the convergent close-coupling (CCC) method has been successfully applied to the study of electron scattering from hydrogen atoms [3], alkali atoms [4], helium atoms [5], and alkali-earth atoms [6]. The ability of the CCC method to accommodate relatively large close-coupling expansions combined together with the account of coupling to the target continuum via its square-integrable representation yields reliable results across a wide spectrum of incident electron energies and scattering processes. The application of the CCC method to electron scattering from heavy atoms, such as cesium [7–9], barium [10], and mercury [11], demonstrated good agreement with experiment but also revealed the limitations of the method. These, first of all, are related to the importance of the relativistic effects both in the description of the heavy atoms target wave functions and scattering dynamics. In particular, experiments with spin-polarized electrons and targets performed by Bielefeld group [7–9] for the electron-cesium scattering system produced differential cross section (DCS) and three spin asymmetries (A_{nn},A_1,A_2). Only the exchange spin asymmetry A_{nn} can be obtained with nonrelativistic methods, with the spin asymmetries A_1 and A_2 being identically zero in such methods. Collectively, these parameters form an ideal test of relativistic approaches and will be used here to check the accuracy of the RCCC method.

It has been recognized for a long time in the field that the most consistent approach to theoretical modeling of electron scattering from heavy atoms should be the one based on a solution of relevant Dirac equations for both target wave functions and electron-atom scattering. A number of theoretical methods are available at present that follow a fully relativistic formulation. The most advanced of them are the Dirac *R*-matrix method [12–15], the recently developed Dirac *B*-spline *R*-matrix method (DBRM) [16,17], and Dirac *R* matrix with pseudostates method (DRMPS) [18]. These calculations are most computationally effective at low energies where the size of the close-coupling expansion does not have to be large to obtain converged results. However, at intermediate energies, a large close-coupling expansion is often required. In a relativistic formulation, the size of the close-coupling expansion is about twice larger than in the corresponding nonrelativistic method which makes the relativistic *R*-matrix calculations computationally difficult to perform [16]. The problem of large close-coupling expansions can be avoided at high incident electron energies where first-order methods can be used. Extensive calculations of electron-atom elastic scattering and excitations have been performed using such first-order techniques (see, for example, Refs. [19,20]).

This paper is organized as follows. In the following section, we describe in detail the RCCC method with emphasis on applications to scattering from quasi-one-electron atoms. The results for *e*-Cs elastic scattering are presented in the next section, followed by conclusions and outlook to future work.

II. THEORY

We assume that the target atom or ion is well described by a model of one electron above a frozen Dirac-Fock core. The set of core orbitals $\{\varphi_c\}$ is obtained by performing a self-consistent field Dirac-Fock calculation using, for example, the GRASP package [21]. The resulting Dirac equation for the active electron wave function is

$$H_T\phi(\boldsymbol{r}) = (c\boldsymbol{\alpha}\cdot\boldsymbol{p} + \beta m_0 c^2 + V_T)\phi(\boldsymbol{r}) = \epsilon\phi(\boldsymbol{r}), \qquad (1)$$

where $\boldsymbol{\alpha}$ and β are the Dirac matrices, c is the speed of light, m_0 is the electron mass, and $\boldsymbol{p}$ is the momentum operator. In what follows, we will use atomic units $m_0=1$ and $c\approx 137$. For a central potential V_T, the solutions of the Dirac equation (1) are characterized by the relativistic quantum number κ and are given by a four-component spinor [22]

*d.fursa@curtin.edu.au

$$\phi_{\kappa m}(\boldsymbol{r}) = \frac{1}{r}\begin{pmatrix} \phi_\kappa^L(r)\chi_{\kappa m} \\ i\phi_\kappa^S(r)\chi_{-\kappa m} \end{pmatrix}. \tag{2}$$

Here, $\phi_\kappa^L(r)$ and $\phi_\kappa^S(r)$ are the large and small components of the radial-wave function, $\chi_{\kappa m}$ is a two-component coupled spin-orbit function, and m is the magnetic quantum number. The relativistic quantum number κ is related to the total angular momentum j and parity $\pi=(-1)^l$ of the orbital via

$$j = |\kappa| - \frac{1}{2}, \tag{3}$$

$$l = \begin{cases} \kappa, & \kappa > 0 \\ -\kappa - 1 & \kappa < 0. \end{cases} \tag{4}$$

The potential V_T of interaction of the active electron with a closed core is a sum of a frozen-core Dirac-Fock potential V^{FC} and a polarization potential V^{pol},

$$V_T = V^{\mathrm{FC}} + V^{\mathrm{pol}}. \tag{5}$$

The nonlocal V^{FC} potential is defined as a sum of local (direct) V_d^{FC} and nonlocal (exchange) terms

$$V_T = V_d^{\mathrm{FC}} + V_e^{\mathrm{FC}}, \tag{6}$$

with

$$V_d^{\mathrm{FC}}\phi(\boldsymbol{r}) = \left(-\frac{Z}{r} + \sum_{\varphi_c}\int d^3r' \frac{|\varphi_c(\boldsymbol{r}')|^2}{|\boldsymbol{r}-\boldsymbol{r}'|}\right)\phi(\boldsymbol{r}), \tag{7}$$

$$V_e^{\mathrm{FC}}\phi(\boldsymbol{r}) = -\sum_{\varphi_c}\int d^3r' \frac{\varphi_c(\boldsymbol{r}')^*\phi(\boldsymbol{r}')}{|\boldsymbol{r}-\boldsymbol{r}'|}\varphi_c(\boldsymbol{r}'). \tag{8}$$

We use a point-nuclear model with Z being the nuclear charge. The number of electrons in the frozen core is $N_c = \Sigma_{\varphi_c}(2j_c+1)$. Note that for neutral atoms $Z=N_c+1$, but for positively charged ions, the asymptotic charge of the target is nonzero

$$Z_{\mathrm{as}} = Z - N_c - 1. \tag{9}$$

The phenomenological one-electron core-polarization potential V^{pol} allows us to take into account more accurately the effect of closed inert shells on the active electron. For light atoms and ions, a simple model used in the nonrelativistic CCC method [4] can be used. However, for heavy targets, such as cesium, a more accurate form of polarization potential is necessary. The polarized-orbital methods of McEachran *et al.* [23] can be used to produce the polarization potential from the core orbitals.

A. Diagonalization of the Dirac Hamiltonian

The key step in the formulation of the CCC method is the diagonalization of the nonrelativistic Schrödinger Hamiltonian of the target in a finite-size Sturmian basis. In the case of the Dirac Hamiltonian, diagonalization in a finite-size basis proved to be a significantly more complicated problem. Firstly, the spectrum of the Dirac Hamiltonian of a hydrogenlike atom does not have a finite lower bound and consists of three distinct intervals: the continuous spectrum $(-\infty, -2c^2)$ corresponding to the negative-energy electrons (positrons), the discrete spectrum $(-2c^2, 0)$ containing the target bound states, and the target continuous spectrum $(0, \infty)$ (see Fig. 1). The absence of the lowest-energy state for the Dirac Hamiltonian means that the variational principle and techniques derived from it such as diagonalization in the finite-size basis cannot be applied to the problem, at least not in the same straightforward manner as is done for the nonrelativistic Schrödinger Hamiltonian. Secondly, the choice of the basis proved to be very important as a simple generalization of the nonrelativistic diagonalization techniques leads to the appearance of so-called "intruder" states [24] that carry no physical meaning and were an artifact of the incorrect account of the interaction between the negative-energy electron continuum and the positive-energy bound and continuum parts of the Dirac equation spectrum.

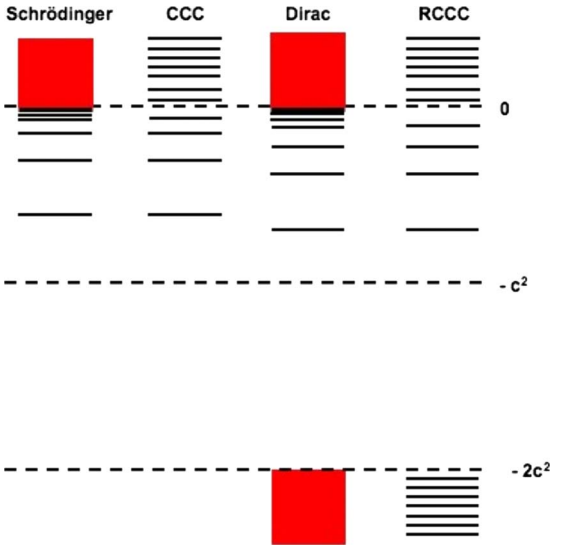

FIG. 1. (Color online) A qualitative comparison of the Dirac and Schrödinger target spectra and their discretization using CCC and RCCC methods. The energy was shifted by $-c^2$ to facilitate comparison to CCC. Note that RCCC generally yields a lower energy ground state.

The problems of the applicability of the variational principle to the Dirac Hamiltonian and choice of the basis for diagonalization were resolved by Grant and Quiney [25] (we refer the reader to this reference for the detailed discussion). We should also note that an alternative but equivalent formulation was presented by Szmytkowski [26]. In this paper, we will follow the formulation of Grant and Quiney [25].

The target atom wave function $\phi_{\kappa m}(\mathbf{r})$ is sought as an expansion [25]

$$\phi_{\kappa m}(\boldsymbol{r}) = \frac{1}{r}\begin{pmatrix} \phi_\kappa^L(r)\chi_{\kappa m} \\ i\phi_\kappa^S(r)\chi_{-\kappa m} \end{pmatrix} = \frac{1}{r}\begin{pmatrix} \sum_{n_r} c_{n_r}^L f_{n_r\kappa}^L(r)\chi_{\kappa m} \\ i\sum_{n_r} c_{n_r}^S f_{n_r\kappa}^S(r)\chi_{-\kappa m} \end{pmatrix}. \tag{10}$$

Here, $c_{n_r}^L$ and $c_{n_r}^S$ are expansion coefficients and $f_{n_r\kappa}^L(r)$ and $f_{n_r\kappa}^S(r)$ are Dirac L spinors [25]. Dirac L spinors form a com-

plete square-integrable basis and are the relativistic analogue of Coulomb Sturmian functions (Laguerre functions) which are used in the formulation of the nonrelativistic CCC method. The important feature of the expansion (10) is that although the large and small components of the wave function are expanded separately, the Dirac L spinors for large and small components are not independent but satisfy the following system of differential equations:

$$\frac{d}{dr}f^L_{n_r\kappa}(r) = -\frac{\kappa}{r}f^L_{n_r}(r) + \left(\frac{N_{n_r\kappa} - n_r - \gamma}{r} + \lambda\right)f^S_{n_r}, \quad (11)$$

$$\frac{d}{dr}f^S_{n_r\kappa}(r) = \frac{\kappa}{r}f^S_{n_r}(r) + \left(\frac{-N_{n_r\kappa} - n_r - \gamma}{r} + \lambda\right)f^L_{n_r}, \quad (12)$$

where $\gamma = \sqrt{\kappa^2 - (Z/c)^2}$ and $N_{n_r\kappa} = \sqrt{\kappa^2 + 2n_r\gamma + n_r^2}$. The consequence of this relation is that the large and small components of the Dirac L spinors satisfy the criterion of strict kinetic balance [25] which guarantees the correct account of the interaction between different parts of the Dirac equation spectrum and the correct transition to the nonrelativistic limit ($c \to \infty$). The explicit form of the Dirac L spinors is

$$f^{L/S}_{n_r\kappa}(r) = \left[\frac{n_r!\,(2\gamma + n_r)}{2N_{n_r\kappa}(N_{n_r\kappa} - \kappa)\Gamma(2\gamma + n_r)}\right]^{1/2}(2\lambda r)^{\gamma}e^{-\lambda r} \times\left(-(1 - \delta_{n_r,0})L^{2\gamma}_{n_r-1}(2\lambda r) \pm \frac{N_{n_r\kappa} - \kappa}{n_r + 2\gamma}L^{2\gamma}_{n_r}(2\lambda r)\right), \quad (13)$$

with the + (−) corresponding to the large (small) components, respectively. $\Gamma(a)$ is the usual gamma function [27]. Dirac L spinors are normalized to unity but form a nonorthogonal set. We refer the reader to Ref. [25] for a detailed discussion of the Dirac L spinor properties, such as orthogonality and the transition to the nonrelativistic limit. We also note that Dirac L spinors have been used to generate a compete set of pseudostates in the DRMPS method [18].

The problem of diagonalization of the Hamiltonian H_T in the basis of L spinors is divided into two steps. In the first step, we consider the Dirac equation (1) with the local part of the potential, $V_T^{\rm loc} = V_d^{\rm FC} + V^{\rm pol}$, and formulate a standard eigenvalue problem for the expansion coefficients $\{c^L_{n_r}, c^S_{n_r}\}, n_r = 1, \ldots, N_\kappa$ by substitution of the expansion (10) into the (local) Dirac equation

$$\sum_{n_r}\langle f^L_{m_r\kappa}|V_T^{\rm loc} + c^2|f^L_{n_r\kappa}\rangle c^L_{n_r} - c\sum_{n_r}\langle f^L_{m_r\kappa}|\frac{d}{dr} - \frac{\kappa}{r}|f^S_{n_r\kappa}\rangle c^S_{n_r} = \sum_{n_r}\epsilon\langle f^L_{m_r\kappa}|f^L_{n_r\kappa}\rangle c^L_{n_r}, \quad (14)$$

$$c\sum_{n_r}\langle f^S_{m_r\kappa}|\frac{d}{dr} + \frac{\kappa}{r}|f^L_{n_r\kappa}\rangle c^L_{n_r} + \sum_{n_r}\langle f^S_{m_r\kappa}|V_T^{\rm loc} - c^2|f^S_{n_r\kappa}\rangle c^S_{n_r} = \sum_{n_r}\epsilon\langle f^S_{m_r\kappa}|f^S_{n_r\kappa}\rangle c^S_{n_r}. \quad (15)$$

Note that for N_κ L spinors used in expansion (10), the size of the eigenvalue problem is $2N_\kappa$. The result of the diagonalization is a set of $2N$ orbitals $\{\tilde{\phi}_n\}$ and corresponding energies $\tilde{\epsilon}_n$ with N_κ of them describing bound states and discretized continuum states for the potential $V_T^{\rm loc}$ and in addition there is a set of N_κ orbitals describing discretized negative-energy continuum states (see Fig. 1). According to Dirac [28], the negative-energy states are filled with electrons and the Pauli exclusion principle prohibits decay to them from positive-energy bound and continuum parts of spectrum. Excitations from the negative-energy states result in the creation of electron-positron pairs. The energy required for such processes ($\sim 2c^2 \approx 1$ MeV) is much higher than the energies normally considered in electron-atom collision studies. Therefore, we will exclude all negative-energy orbitals that come from the diagonalization of the Dirac Hamiltonian.

In the second step, we use N_κ (positive-energy) orbitals $\{\tilde{\phi}_n\}$ as a basis to diagonalize the full-target Hamiltonian H_T. This requires evaluation of the matrix elements of the nonlocal frozen-core potential $V_e^{\rm FC}$,

$$\langle\tilde{\phi}_n|V_e^{\rm FC}|\tilde{\phi}_{n'}\rangle = \delta_{\kappa_n,\kappa_{n'}}\sum_{\varphi_c}\sum_{\lambda}\frac{2j_c + 1}{2j_n + 1}\Pi(\kappa_n, \kappa_c, \lambda) \times (C^{j_n 1/2}_{j_c 1/2,\lambda 0})^2\int_0^\infty dr'\,\varphi_c(r')\tilde{\phi}_n(r') \times\int_0^\infty dr\varphi_c(r)\tilde{\phi}_n(r), v_\lambda(r', r), \quad (16)$$

where

$$v_\lambda(r', r) = \begin{cases} r^\lambda/r'^{\lambda+1} & \text{for} \quad r' > r \\ r'^\lambda/r^{\lambda+1} & \text{for} \quad r' < r \end{cases} \quad (17)$$

and $\Pi(\kappa_n, \kappa_c, \lambda)$ incorporates the parity selection rules [29]

$$\Pi(\kappa_n, \kappa_c, \lambda) = \frac{1}{2}\left(1 - \frac{\kappa_n}{|\kappa_n|}\frac{\kappa_c}{|\kappa_c|}(-1)^{j_n + j_c + \lambda}\right). \quad (18)$$

The result of the target structure calculations is a set of wave functions $\{\phi^N_n\}$ and corresponding energies ϵ^N_n, $n = 1, \ldots, N = \Sigma_\kappa N_\kappa$, that describe the target atom or ion and satisfy

$$\langle\phi^N_m|H_T|\phi^N_n\rangle = \epsilon^N_n\delta_{m,n}. \quad (19)$$

B. Relativistic scattering formulation

We now turn to the formulation of the relativistic scattering problem. This formulation is similar to the nonrelativistic case and we present here only the main results with emphasis on the differences with the nonrelativistic case [30]. In what follows, we use index "1" to describe the projectile electron coordinates and index "2" for the target electron coordinates.

The Dirac Hamiltonian describing the total projectile electron and target scattering system is given by

$$H = H_1 + H_2 + V_{12}, \quad (20)$$

where $H_i = K_i + V_i$, with K_i denoting the free Dirac Hamiltonian and $V_i = V_i^{\rm FC} + V_i^{\rm pol}$ denoting the interaction potential of electron i with the closed frozen core as described in the

previous section. We note that with this notation, $H_T=H_2$ and $V_T=V_2$. The potential V_{12} denotes the Coulomb electron-electron potential. Generalization to the Breit and Møller potentials will be discussed elsewhere.

The total scattering wave function satisfies

$$(E-H)|\Psi_i^{(+)}\rangle = 0, \tag{21}$$

where the superscript (+) denotes incoming plane- or Coulomb-wave and outgoing spherical-wave boundary conditions and the initial target state is ϕ_i and projectile momentum is k_i.

We use the set of target states $\{\phi_n^N\}$ to perform a multichannel expansion of the total wave function

$$|\Psi_i^{N(+)}\rangle = \frac{1}{2}(1-P_{12})|\psi_i^{N(+)}\rangle = \frac{1}{2}(1-P_{12})\sum_n |f_{n,i}^N \phi_n^N\rangle, \tag{22}$$

where $f_{n,i}^N$ are channel functions and P_{12} is the space exchange operator. The explicit antisymmetrization in Eq. (22) guarantees that the total wave function satisfies the Pauli exclusion principle

$$\langle x_1 x_2|\Psi_i^{N(+)}\rangle = -\langle x_2 x_1|\Psi_i^{N(+)}\rangle. \tag{23}$$

However, it leads to nonunique channel functions $f_{n,i}^N$ and consequently to an ill-defined set of scattering equations. Similarly to the nonrelativistic case, one can show that uniqueness of the total wave function can be ensured, without loss of generality, by imposing the following condition:

$$\langle \phi_m^N|f_{n,i}^N\rangle = -\langle \phi_n^N|f_{m,i}^N\rangle. \tag{24}$$

We now turn to the derivation of the close-coupling equations. In the general case, the charged target has asymptotic charge $Z_{\rm as}$ [see Eq. (9)] with the asymptotic Hamiltonian of the scattering system defined as

$$H_{\rm as} = K_1 - \frac{Z_{\rm as}}{r_1} + H_2. \tag{25}$$

The distorted waves $|\boldsymbol{k}^{(\pm)},\mu,b\rangle$ are solutions of the one-electron Dirac equation

$$\left(\epsilon - K_1 + \frac{Z_{\rm as}}{r_1} - U_1\right)|\boldsymbol{k}^{(\pm)},\mu,b\rangle = 0, \tag{26}$$

where U_1 is an arbitrary short-ranged distorting potential, μ is the spin magnetic number, and b is the sign of energy, $\epsilon = \pm\epsilon_k = \pm c\sqrt{k^2+c^2}$, with the positive sign corresponding to electrons and the negative sign to positrons (negative-energy electrons). The Dirac distorted-waves satisfy the following orthogonality and completeness conditions:

$$\langle \boldsymbol{k}^{(\pm)}\mu b|\boldsymbol{k}'^{(\pm)}\mu' b'\rangle = \delta_{\mu,\mu'}\delta_{b,b'}\delta(\boldsymbol{k}-\boldsymbol{k}'), \tag{27}$$

$$\sum\!\!\!\!\!\!\int_{b\mu} d^3k |\boldsymbol{k}^{(\pm)}\mu b\rangle\langle \boldsymbol{k}^{(\pm)}\mu b| = \tilde{1}, \tag{28}$$

where $\tilde{1}$ denotes the unity 4×4 matrix.

Dirac distorted waves reduce to standard Dirac plane waves in the case of scattering from neutral targets and zero distorting potential and are given by [31]

$$|\boldsymbol{k}\mu b\rangle = U_\mu^b|\boldsymbol{k}\rangle = U_\mu^b \frac{1}{(2\pi)^{3/2}} e^{i\boldsymbol{k}\cdot\boldsymbol{r}}, \tag{29}$$

where the four-component spinors U_μ^b are

$$U_\mu^+ = \sqrt{\frac{\epsilon_k + c^2}{2\epsilon_k}}\begin{pmatrix} \chi_\mu \\ \dfrac{c\boldsymbol{\sigma}\cdot\boldsymbol{k}}{\epsilon_\kappa + c^2}\chi_\mu \end{pmatrix}, \tag{30}$$

$$U_\mu^- = \sqrt{\frac{\epsilon_k + c^2}{2\epsilon_k}}\begin{pmatrix} -\dfrac{c\boldsymbol{\sigma}\cdot\boldsymbol{k}}{\epsilon_k + c^2}\chi_\mu \\ \chi_\mu \end{pmatrix}.$$

Here, $\boldsymbol{\sigma}$ consists of the Pauli matrices and χ_μ are two-component basis spinors.

The spectral decomposition of the Dirac Green's function,

$$G^{(\pm)}(E) = \sum_\mu \sum\!\!\!\!\!\!\int d^3k \left(\frac{|\boldsymbol{k}^{(\pm)}\mu+\rangle\langle \boldsymbol{k}^{(\pm)}\mu+|}{E-\epsilon_k \pm i0} + \frac{|\boldsymbol{k}^{(\pm)}\mu-\rangle\langle \boldsymbol{k}^{(\pm)}\mu-|}{E+\epsilon_k \pm i0}\right), \tag{31}$$

has now two terms corresponding to the positive-energy and negative-energy parts of the spectrum.

Substituting the expansion (22) in the Dirac equation (21), we obtain

$$(E-H_{\rm as}-U_1)|\psi^{N(+)}\rangle = \left(V_1 + \frac{Z_a}{r_1} - U_1 + V_{12} + [E-H]P_{12}\right)\times|\psi^{N(+)}\rangle, \tag{32}$$

Using the Green's function (31), we can transform Eq. (32) to the momentum-space Lippmann-Schwinger equation

$$|\psi^{N(+)}\rangle = |\boldsymbol{k}_i^{(+)}\mu_i b_i \phi_i^N\rangle + \sum_n \sum\!\!\!\!\!\!\int_{b,\mu} dk^3 \frac{|\boldsymbol{k}^{(-)}\mu b\phi_n\rangle\langle \boldsymbol{k}^{(-)}\mu b\phi_n^N|V_U|\psi_S^{(+)}\rangle}{E-\epsilon_n^N - b\epsilon_k + i0}. \tag{33}$$

Here, $|\boldsymbol{k}^{(+)}\mu b\phi\rangle = |\boldsymbol{k}^{(+)}\mu b\rangle|\phi\rangle$ and

$$V_U^N = V_1 + \frac{Z_a}{r_1} - U_1 + V_{12} - E\theta I_1^N + [E(1-\theta)-H]P_{12}. \tag{34}$$

Any nonzero constant θ implements the condition (24) (see Refs. [4,32] for details).

We premultiply Eq. (33) by $\langle \boldsymbol{k}_f^{(-)}\mu_f b_f \phi_f^N|V_U^N$ to obtain a set of Lippmann-Schwinger equations,

$$T_{fi}^{++}(\boldsymbol{k}_f^{(-)}\mu_f,\boldsymbol{k}_i^{(+)}\mu_i) = V_{fi}^{++}(\boldsymbol{k}_f^{(-)}\mu_f,\boldsymbol{k}_i^{(+)}\mu_i) + \sum_{n=1}^{N}\sum_{\mu}\oint d^3k \frac{V_{fn}^{++}(\boldsymbol{k}_f^{(-)}\mu_f,\boldsymbol{k}^{(-)}\mu)T_{ni}^{++}(\boldsymbol{k}^{(-)}\mu,\boldsymbol{k}_i^{(+)}\mu_i)}{E-\epsilon_n-\epsilon_k+i0}$$
$$+\sum_{n=1}^{N}\sum_{\mu}\oint d^3k \frac{V_{fn}^{+-}(\boldsymbol{k}_f^{(-)}\mu_f,\boldsymbol{k}^{(-)}\mu)T_{ni}^{-+}(\boldsymbol{k}^{(-)}\mu,\boldsymbol{k}_i^{(+)}\mu_i)}{E-\epsilon_n+\epsilon_k+i0}, \tag{35}$$

$$T_{fi}^{-+}(\boldsymbol{k}_f^{(-)}\mu_f,\boldsymbol{k}_i^{(+)}\mu_i) = V_{fi}^{-+}(\boldsymbol{k}_f^{(-)}\mu_f,\boldsymbol{k}_i^{(+)}\mu_i) + \sum_{n=1}^{N}\sum_{\mu}\oint d^3k \frac{V_{fn}^{-+}(\boldsymbol{k}_f^{(-)}\mu_f,\boldsymbol{k}^{(+)}\mu)T_{ni}^{++}(\boldsymbol{k}^{(-)}\mu,\boldsymbol{k}_i^{(+)}\mu_i)}{E-\epsilon_n-\epsilon_k+i0}$$
$$+\sum_{n=1}^{N}\sum_{\mu}\oint d^3k \frac{V_{fn}^{--}(\boldsymbol{k}_f^{(-)}\mu_f,\boldsymbol{k}_\mu^{(-)})T_{ni}^{-+}(\boldsymbol{k}^{(-)}\mu,\boldsymbol{k}_i^{(+)}\mu_i)}{E-\epsilon_n+\epsilon_k+i0}, \tag{36}$$

where the T-matrix elements are defined as

$$T_{fi}^{b_f b_i}(\boldsymbol{k}_f^{(-)}\mu_f,\boldsymbol{k}_i^{(+)}\mu_i) = \langle \boldsymbol{k}_f^{(-)}\mu_f b_f \phi_f^N | T_U^N | \boldsymbol{k}_i^{(+)}\mu_i b_i \phi_i\rangle$$
$$= \langle \boldsymbol{k}_f^{(-)}\mu_f b_f \phi_f^N | V_U^N | \Psi_i^{(+)}\rangle \tag{37}$$

and

$$V_{nn'}^{bb'}(\boldsymbol{k}^{(\pm)}\mu,\boldsymbol{k}'^{(\pm)}\mu') = \langle \boldsymbol{k}^{(\pm)}\mu b \phi_n^N | V_U^N | \boldsymbol{k}'^{(\pm)}\mu' b' \phi_{n'}^N\rangle. \tag{38}$$

Note that for clarity, we dropped indexes N and U.

The T-matrix element $T_{ni}^{-+}(\boldsymbol{k}\mu,\boldsymbol{k}_i\mu_i)$ describes transition from a positive-energy state to a negative-energy state. The important feature of the Lippmann-Schwinger equation (36) is that the projectile electron negative-energy states enter the equation only as virtual states. For a positive total energy E of the scattering system, the Green's function associated with the negative-energy term $T_{ni}^{-+}(\boldsymbol{k}\mu,\boldsymbol{k}_i\mu_i)$ has no singularity $(E-\epsilon_n+\epsilon_k>0$, i.e., we assume here that the energies of target bound states are much less than the electron rest energy) and therefore it describes closed states. In what follows, we drop all negative-energy terms in the Lippmann-Schwinger equation. For electron-atom or -ion scattering processes, the error associated with this approximation is negligible as the Green's function for the negative-energy terms is of order $1/2c^2$. The resulting form of the Lippmann-Schwinger equation is the same as for the nonrelativistic case and involves transitions between positive-energy states only, however, it contains relativistic kinematics. Exclusion of the negative-energy states in both target structure and scattering formulation is equivalent to the so-called no-virtual-pair approximation [33,34].

The following choice for the distorting potential U has been used in our calculations:

$$U(r) = V^{\mathrm{pol}}(r) - \frac{N_c+1}{r} + \sum_{\varphi_c}\int d^3r' \frac{|\varphi_c(\boldsymbol{r}')|^2}{|\mathbf{r}-\boldsymbol{r}'|}$$
$$+\int d^3r' \frac{|\phi_n(\boldsymbol{r}')|^2}{|\boldsymbol{r}-\boldsymbol{r}'|}, \tag{39}$$

where we typically take ϕ_n to be the ground state. This choice leads to a short-ranged potential while at the same time it allows us to minimize the numerical problems arising from large Z/r terms in V-matrix elements. Finally, we note that similar to the nonrelativistic CCC method [4], the physical T matrix $(U=0)$ can be extracted from the distorted-wave T matrix via

$$\langle \boldsymbol{k}_f^{(-)}\mu_f + \phi_f^N | T | \boldsymbol{k}_i^{(+)}\mu_i + \phi_i\rangle = \langle \boldsymbol{k}_f^{(-)}\mu_f + \phi_f^N | T_U | \boldsymbol{k}_i^{(+)}\mu_i + \phi_i\rangle$$
$$+ \langle \boldsymbol{k}_f^{(-)}\mu_f + | U | \boldsymbol{k}_i^{(+)}\mu_i + \rangle \delta_{f,i}, \tag{40}$$

where the absence of index U in the left-hand side indicates that the final T matrix must be independent of the choice of this distorting potential.

C. Partial wave expansion

The Lippmann-Schwinger equation for the partial-wave T matrix can be obtained from Eq. (36) by performing a partial-wave expansion of the T matrix and V matrix. In order to do this, we need to specify a partial-wave representation of the (positive-energy) Dirac distorted waves [35]

$$|\boldsymbol{k}^{(\pm)}\mu+\rangle = \sqrt{\frac{\epsilon_k+c^2}{\pi\epsilon_k}}$$
$$\times \sum_{\kappa,m} i^L C_{Lm-\mu,1/2\mu}^{jm} Y_L^{*m-\mu}(\boldsymbol{k}) e^{\pm i(\sigma_\kappa+\delta_\kappa)} \frac{1}{kr} |u_{\kappa,k}^m\rangle, \tag{41}$$

where $C_{j_1m_1,j_2m_2}^{jm}$ is a Clebsch-Gordan coefficient, σ_κ is the Dirac-Coulomb phase shift, δ_κ is the distorted-wave phase shift, $j=|\kappa|-1/2$, and

$$\langle \boldsymbol{r} | u_{\kappa,k}^m\rangle = \begin{pmatrix} u_{k\kappa}^L(r)\chi_{\kappa m} \\ i u_{k\kappa}^S(r)\chi_{-\kappa m}\end{pmatrix}. \tag{42}$$

The radial functions $u_{k\kappa}^{L/S}(r)$ are calculated numerically using an Adams-Moulton predictor-corrector integration method as described by Sienkiewicz and Baylis [36]. In Eq. (41), the normalization of the radial function $u_{k\kappa}^{L/S}(r)$ is chosen such that at large values of r, the radial function oscillates with unit amplitude and has the following asymptotic form:

$$u_{k\kappa}^{L/S}(r) \sim \cos(\delta_\kappa) F_\kappa^{L/S}(kr) + \sin(\delta_\kappa) G_\kappa^{L/S}(kr), \quad (43)$$

where $F^{L/S}$ and $G^{L/S}$ are the regular and irregular Dirac-Coulomb functions, respectively. We use the program DCOUL of Salvat *et al.* [37] to calculate Dirac-Coulomb phase shifts σ_κ. The same program is also used to find values of the Dirac-Coulomb functions in the asymptotic region ($U=0$) in order to determine distorted-wave phase shifts δ_κ and to choose the correct normalization of the $u_{k\kappa}^{L/S}(r)$ functions.

The partial-wave expansion of the V and T matrices can now be defined as

$$\begin{aligned}\langle k^{(-)}\kappa, n{:}\Pi J|V|k'^{(+)}\kappa', n'{:}\Pi J\rangle &= \sum_{M\mu m_n M'\mu' m_{n'}} C^{jm_j}_{LM,1/2\mu} C^{j'm'_j}_{L'M',1/2\mu'} C^{JM_J}_{jm_j j_n m_n} C^{JM_J}_{j'm'_j j_{n'} m_{n'}} \\ &\times \int d\boldsymbol{k} \int d\boldsymbol{k}' Y_L^{*M}(\hat{\boldsymbol{k}}) Y_{L'}^{M'}(\hat{\boldsymbol{k}}') \langle \boldsymbol{k}^{(-)}\mu +, \phi_n^N|V|\boldsymbol{k}'^{(+)} \\ &\times \mu' +, \phi_{n'}^N\rangle, \end{aligned} \quad (44)$$

where J and M_J are the total angular momentum of the scattering system and its projection, $\Pi=\pi(-1)^L=\pi'(-1)^{L'}$ is the total parity, and $|k\kappa, n{:}\Pi J\rangle$ stands for the angular-momentum-coupled projectile-target wave function. The partial-wave V matrix (44) is complex, but a real quantity can be defined via

$$\begin{aligned} V^{\Pi J}_{n,n'}(k\kappa, k'\kappa') &= (i)^L(-i)^{L'} \\ &\times e^{-i\eta} e^{-i\eta'} \langle k^{(-)}\kappa, n{:}\Pi J|V|k'^{(+)}\kappa', n'{:}\Pi J\rangle, \end{aligned} \quad (45)$$

where $\eta_\kappa=\sigma_\kappa+\delta_\kappa$. The V-matrix elements (45) can be easily evaluated using standard techniques of relativistic atomic structure [29,34]. Adopting for the partial-wave T matrix the same definition as in Eq. (45), the Lippmann-Schwinger equation (36) reduces to the following partial-wave form:

$$\begin{aligned} T^{\Pi J}_{fi}(k_f\kappa_f, k_i\kappa_i) &= V^{\Pi J}_{fi}(k_f\kappa_f, k_i\kappa_i) \\ &+ \sum_n \sum_\kappa \oint k^2 dk \frac{V^{\Pi J}_{fn}(k_f\kappa_f, k\kappa) T^{\Pi J}_{ni}(k\kappa, k_i\kappa_i)}{E - \epsilon_n^N - \epsilon_{k'} + i0}. \end{aligned} \quad (46)$$

This equation can be solved numerically using complex arithmetic. However, we find it more convenient to define a real K matrix and solve the corresponding set of equations in real arithmetic. The transformation from the complex T matrix to real K matrix is similar to the nonrelativistic case

$$\begin{aligned} K^{\Pi J}_{ni}(k_n\kappa, k_i\kappa_i) &= \sum_{\kappa'} \sum_{n'=1}^{N_o} T^{\Pi J}_{nn'}(k_n\kappa, k_{n'}\kappa') \\ &\times (\delta_{n',i}\delta_{\kappa',\kappa_i} + i\pi\mu_{n'} K^{\Pi J}_{n'i}(k_{n'}\kappa', k_i\kappa_i)), \end{aligned} \quad (47)$$

where N_o specifies the number of open channels for which $\epsilon_{k_n}=E-\epsilon_n>0$ and

$$\mu_n = k_n \frac{\epsilon_{k_n}}{c^2}. \quad (48)$$

The difference compared to the nonrelativistic result ($\mu_n=k_n$) comes from the difference in the relation between energy and momentum in relativistic and nonrelativistic theory. The Lippmann-Schwinger equation for the K matrix can be written as

$$\begin{aligned} K^{\Pi J}_{fi}(k_f\kappa_f, k_i\kappa_i) &= V^{\Pi J}_{fi}(k_f\kappa_f, k_i\kappa_i) \\ &+ \sum_n \sum_\kappa \mathrm{P} \oint k^2 dk \frac{V^{\Pi J}_{fn}(k_f\kappa_f, k\kappa) K^{\Pi J}_{ni}(k\kappa, k_i\kappa_i)}{E - \epsilon_n^N - \epsilon_{k'}}, \end{aligned} \quad (49)$$

where P stands for a principal-value integral. The V matrix in the above equation is real and symmetric which leads to the real and symmetric K matrix.

The important advantage of obtaining the T matrix via Eq. (47) is that the resultant T matrix is symmetric and unitary by construction

$$\begin{aligned} \mathrm{Im}[T^{\Pi J}_{fi}(k_f\kappa_f, k_i\kappa_i)] &= -\pi \sum_n \sum_{\kappa_n} \mu_n T^{*\Pi J}_{fn}(k_f\kappa_f, k_n\kappa_n) T^{\Pi J}_{ni}(k_n\kappa_n, k_i\kappa_i). \end{aligned} \quad (50)$$

The coupled set of integral equations (49) is solved for each value of total parity Π and angular momentum J by replacing integration over momentum by a quadrature rule. The choice of quadrature rule and reduction to the set of linear equations is practically the same as in the nonrelativistic CCC method [4,30].

D. Scattering amplitude and cross section

We define the scattering amplitude $F^{\mu_f\mu_i}_{fi}(\theta)$ in the collision frame (z axis is along the incident momentum of the projectile and θ is the angle between scattered electron momentum and z axis) for a transition from a state ϕ_i with parity π_i, angular momentum j_i, its projection m_i to a state ϕ_f with parity π_f, angular momentum j_f, its projection m_f as

$$\begin{aligned} F^{\mu_f\mu_i}_{m_f m_i}(\theta) &= -\sum_{\kappa_f\kappa_i J\Pi} i^{L_i - L_f} e^{\eta_{\kappa_f} + \eta_{\kappa_i}} C^{jm_i}_{L_f M_f, 1/2\mu_f} C^{j'\mu_i}_{L_i 0, 1/2\mu_i} \\ &\times C^{JM_J}_{jm_j j_f m_f} C^{JM_J}_{j'\mu_i j_i m_i} Y^{M_f}_{L_f}(\hat{\boldsymbol{k}}_f) \sqrt{\frac{2L_i+1}{4\pi}} T^{\Pi J}_{fi}(k_f\kappa_f, k_i\kappa_i), \end{aligned} \quad (51)$$

where $m_j=m_i+\mu_i-m_f$ and $M_f=m_j-\mu_f$. The differential cross section corresponding to the transition described by the scattering amplitude (51) for the case of unpolarized target atom and electron beams can be obtained as

$$\frac{d\sigma_{fi}}{d\Omega} = (2\pi)^4 \frac{k_f}{k_i} \frac{\epsilon_f \epsilon_i}{c^4} \frac{1}{2(2j_i+1)} \sum_{\mu_f\mu_i m_f m_i} |F^{\mu_f\mu_i}_{m_f m_i}(\theta)|^2. \quad (52)$$

Compared to the nonrelativistic case, it has an additional term $\epsilon_f\epsilon_i/c^4$ which appears due to the relativistic relationship between the velocity and momentum [38].

The cross section integrated over electron-scattering angles is given by

$$\sigma_{fi} = \int d\Omega \frac{d\sigma_{fi}}{d\Omega} = \sum_{J\Pi} \sigma_{fi}^{J\Pi}, \tag{53}$$

where the partial-wave integrated cross sections $\sigma_{fi}^{J\Pi}$ can be expressed via the partial-wave T matrix as

$$\sigma_{fi}^{J\Pi} = (2\pi)^4 \frac{k_f}{k_i} \frac{\epsilon_f \epsilon_i}{c^4} \frac{1}{2(2j_i+1)} \frac{2J+1}{4\pi} \sum_{\kappa_f \kappa_i} |T_{fi}^{J\Pi}(k_f\kappa_f, k_i\kappa_i)|^2. \tag{54}$$

For scattering from neutral targets, the unitarity of the T matrix (50) leads to the optical theorem that relates the elastic forward-scattering amplitude and total scattering cross section for a target atom in the initial state with magnetic sublevel m_i and incident electron with spin projection μ_i,

$$\sigma_{m_i\mu_i}^{\text{tot}} = \sum_f \sigma_{m_i\mu_i}^f = (2\pi)^4 \frac{1}{k_i} \frac{\epsilon_i}{c^2} \frac{1}{\pi} \text{Im}[F_{m_i m_i}^{\mu_i \mu_i}(0)], \tag{55}$$

where

$$\sigma_{m_i\mu_i}^f = (2\pi)^4 \frac{k_f}{k_i} \frac{\epsilon_f \epsilon_i}{c^4} \sum_{\mu_f m_f} \int d\Omega |F_{m_f m_i}^{\mu_f \mu_i}(\theta)|^2. \tag{56}$$

The scattering of polarized electrons from polarized Cs atoms has been studied in a series of experiments conducted by the Bielefeld group [7]. These experiments measured the scattered electron intensities for all four possible combinations of relative polarization (with respect to the scattering plane) of incident electron (up or down) and target Cs atom (up and down). This makes it possible to determine the DCS for scattering of unpolarized electrons and target Cs atoms, as well as three spin asymmetries describing scattering of unpolarized electrons from polarized Cs atoms (A_1), polarized electrons from unpolarized atoms (A_2), and "antiparallel-parallel" asymmetry (A_{nn}) for scattering of polarized electrons from polarized Cs atoms. Asymmetries A_1 and A_2 are zero in nonrelativistic calculations and offer a sensitive test to account for relativistic effects in theoretical models. We also note that all spin asymmetries are zero when calculated in the first Born approximation, providing, therefore, a test for importance of channel coupling in e-Cs scattering.

The spin asymmetry parameters A_i can be expressed in terms of differential cross sections in the following way [39]:

$$A_1 = \left[q\left(\frac{1}{2},\frac{1}{2}\right) + q\left(\frac{1}{2},-\frac{1}{2}\right) - q\left(-\frac{1}{2},\frac{1}{2}\right) - q\left(-\frac{1}{2},-\frac{1}{2}\right) \right] / 4q_u, \tag{57}$$

$$A_2 = \left[q\left(\frac{1}{2},\frac{1}{2}\right) + q\left(-\frac{1}{2},\frac{1}{2}\right) - q\left(\frac{1}{2},-\frac{1}{2}\right) - q\left(-\frac{1}{2},-\frac{1}{2}\right) \right] / 4q_u, \tag{58}$$

$$A_{nn} = \left[q\left(\frac{1}{2},-\frac{1}{2}\right) + q\left(-\frac{1}{2},\frac{1}{2}\right) - q\left(\frac{1}{2},\frac{1}{2}\right) - q\left(-\frac{1}{2},-\frac{1}{2}\right) \right] / 4q_u, \tag{59}$$

where the magnetic sublevel DCS is defined as

$$q(m_i\mu_i) = (2\pi)^4 \frac{k_f}{k_i} \frac{\epsilon_f \epsilon_i}{c^4} \sum_{\mu_f m_f} |F_{m_f m_i}^{\mu_f \mu_i}(\theta)|^2, \tag{60}$$

with

$$q_u(\theta) = \frac{d\sigma}{d\Omega} = \frac{1}{4}\left[q\left(\frac{1}{2},-\frac{1}{2}\right) + q\left(-\frac{1}{2},\frac{1}{2}\right) + q\left(\frac{1}{2},\frac{1}{2}\right) + q\left(-\frac{1}{2},-\frac{1}{2}\right) \right]. \tag{61}$$

E. Scattering amplitude and the analytical Born subtraction technique

In any practical calculation, the partial-wave expansion has to be terminated at some value of total angular momentum $J_{\max}$. At high incident electron energies, the $J_{\max}$ value has to be sufficiently large in order to achieve convergence in the partial-wave expansion. We can use the analytical Born subtraction technique to reduce the size of the partial-wave expansion. This technique has been widely used in nonrelativistic electron-atom scattering methods (see, for example, Inokuti [40]), but probably it is less common in the relativistic techniques though recently Fontes and Zhang [41] provided a useful review of it. The analytical Born subtraction technique relies on the property that at large values of total angular momentum J, the partial-wave T matrix becomes equal to the partial-wave V matrix

$$T_{fi}^{J\Pi}(k_f\kappa_f, k_i\kappa_i) = \tilde{V}_{fi}^{J\Pi}(k_f\kappa_f, k_i\kappa_i), \tag{62}$$

where the partial-wave $\tilde{V}$ matrix is calculated with the direct only part of the potential (34),

$$\tilde{V} = V_1 + \frac{Z_{\text{as}}}{r_1} + V_{12}, \tag{63}$$

using Dirac plane waves (29). This is equivalent to calculating the T matrix in the first-order Born approximation (FBA) for the large J values. The above expression holds for scattering from both neutral and charged targets as the centrifugal term becomes dominant at large values of J.

In order to take advantage of the relation (62), we redefine the scattering amplitude (51) as

$$F_{m_f m_i}^{\mu_f \mu_i}(\theta) = -\sum_{\kappa_f \kappa_i J\Pi} C_{L_f M_f, 1/2\mu_f}^{jm_j} C_{L_i 0, 1/2\mu_i}^{j'\mu_i} C_{jm_j, j_f m_f}^{JM_J} \times C_{j'\mu_i, j_i m_i}^{JM_J} i^{L_i - L_f} e^{\eta_{\kappa_f} + \eta_{\kappa_i}} Y_{L_f}^{M_f}(\hat{\boldsymbol{k}}_f) \sqrt{\frac{2L_i+1}{4\pi}} \times [T_{fi}^{J\Pi}(k_f\kappa_f, k_i\kappa_i) - V_{fi}^{J\Pi}(k_f\kappa_f, k_i\kappa_i)] - \langle \boldsymbol{k}_f \mu_f +, \phi_f | \tilde{V} | k_i \mu_i +, \phi_i \rangle. \tag{64}$$

Calculation of cross sections and other scattering parameters discussed in the previous section with use of the amplitude (64) normally does not require a large partial-wave expansion leading to substantial saving in computer time.

Calculation of the scattering amplitude via Eq. (64) requires evaluation of the FBA plane-wave V matrix which can be done using the expressions for the Dirac plane waves (29)

$$\langle \boldsymbol{k}_f \mu_f +, \phi_f | \tilde{V} | \boldsymbol{k}_i \mu_i +, \phi_i \rangle = A_{\mu_f \mu_i}(\theta) \frac{1}{(2\pi)^3} \frac{4\pi}{q^2} R_{m_f m_i}(\theta), \tag{65}$$

where $\boldsymbol{q}=\boldsymbol{k}_i-\boldsymbol{k}_f$ is the momentum transfer,

$$R_{m_f m_i}(\theta) = \langle \phi_f | e^{i\boldsymbol{q}\cdot\boldsymbol{r}} | \phi_i \rangle - \delta_{f,i} \times \left[1 - \int d^3 r_1 e^{i\boldsymbol{q}\cdot\boldsymbol{r}} \left(V_d^{\mathrm{FC}}(r) + \frac{Z_{\mathrm{as}}+1}{r} \right) \right], \tag{66}$$

$$A_{\mu_f \mu_i}(\theta) = U^{+\dagger}_{\mu_f} U^{+}_{\mu_i} = N_{fi} \left[\delta_{\mu_f,\mu_i} \left(1 + \frac{c^2 k_i k_f \cos\theta}{(\epsilon_f + c^2)(\epsilon_i + c^2)} \right) + \delta_{-\mu_f,\mu_i} \frac{2\mu_f c^2 k_i k_f \sin\theta}{(\epsilon_f + c^2)(\epsilon_i + c^2)} \right], \tag{67}$$

and

$$N_{fi} = \sqrt{\left(\frac{\epsilon_i + c^2}{2\epsilon_i} \right) \left(\frac{\epsilon_f + c^2}{2\epsilon_f} \right)}. \tag{68}$$

The DCS calculated using the FBA amplitude leads to

$$\frac{d\sigma_{fi}^{\mathrm{FBA}}}{d\Omega} = \frac{k_f}{k_i} \frac{\epsilon_f \epsilon_i}{c^4} \frac{1}{2j_i+1} \frac{4}{q^4} \sum_{m_f m_i} |R_{m_f m_i}(\theta)|^2 \sum_{\mu_f \mu_i} \frac{1}{2} A_{\mu_f \mu_i}(\theta), \tag{69}$$

with

TABLE I. Ionization energies (eV) of Cs bound low-lying states (relative to the Cs^+ ground state) in the RCCC calculations. Experimental data are from Moore [46].

	RCCC	Experiment
$6s_{1/2}$	3.893	3.893
$6p_{1/2}$	2.509	2.507
$6p_{3/2}$	2.444	2.439
$5d_{3/2}$	2.265	2.096
$5d_{5/2}$	2.260	2.084
$7s_{1/2}$	1.594	1.595
$7p_{1/2}$	1.195	1.195
$7p_{3/2}$	1.174	1.173
$6d_{3/2}$	1.135	1.093
$6d_{5/2}$	1.131	1.088
$4f_{5/2}$	0.859	0.860
$4f_{7/2}$	0.859	0.860

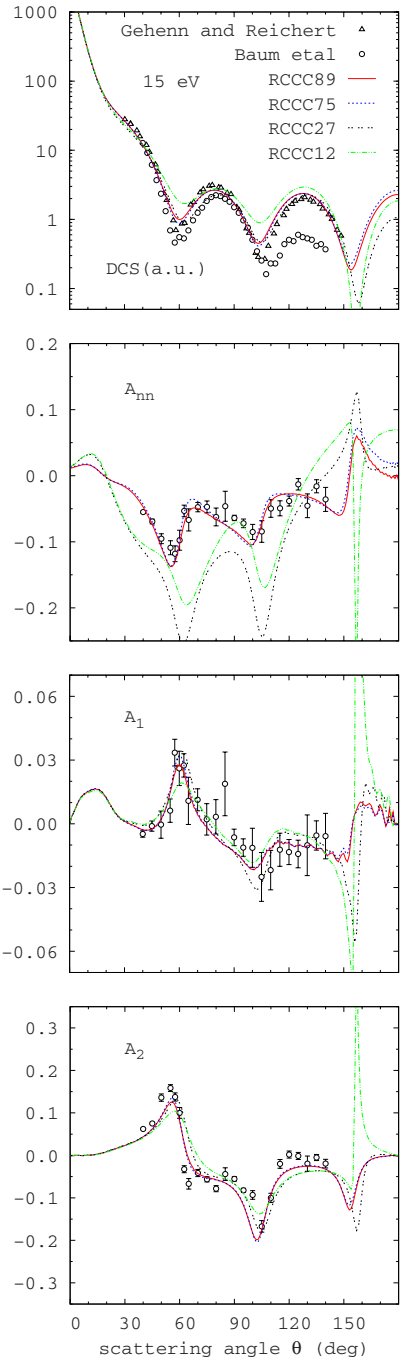

FIG. 2. (Color online) Differential cross sections and spin asymmetries for elastic electron scattering on the ground state of Cs at 15 eV incident electron energy. Convergence of DCS and spin asymmetries is illustrated by performing 12-, 27-, 75-, and 89-state RCCC calculations. Experiment is due to Gehenn and Reichert [43] and Baum *et al.* [7].

$$\sum_{\mu_f \mu_i} \frac{1}{2} A_{\mu_f \mu_i}(\theta) = \frac{1}{2\epsilon_f \epsilon_i} (\epsilon_f \epsilon_i + c^4 + c^2 k_f k_i \cos\theta). \tag{70}$$

In the case of elastic scattering, $k_f=k_i$, the last expression leads to the well-known Mott elastic-scattering formula.

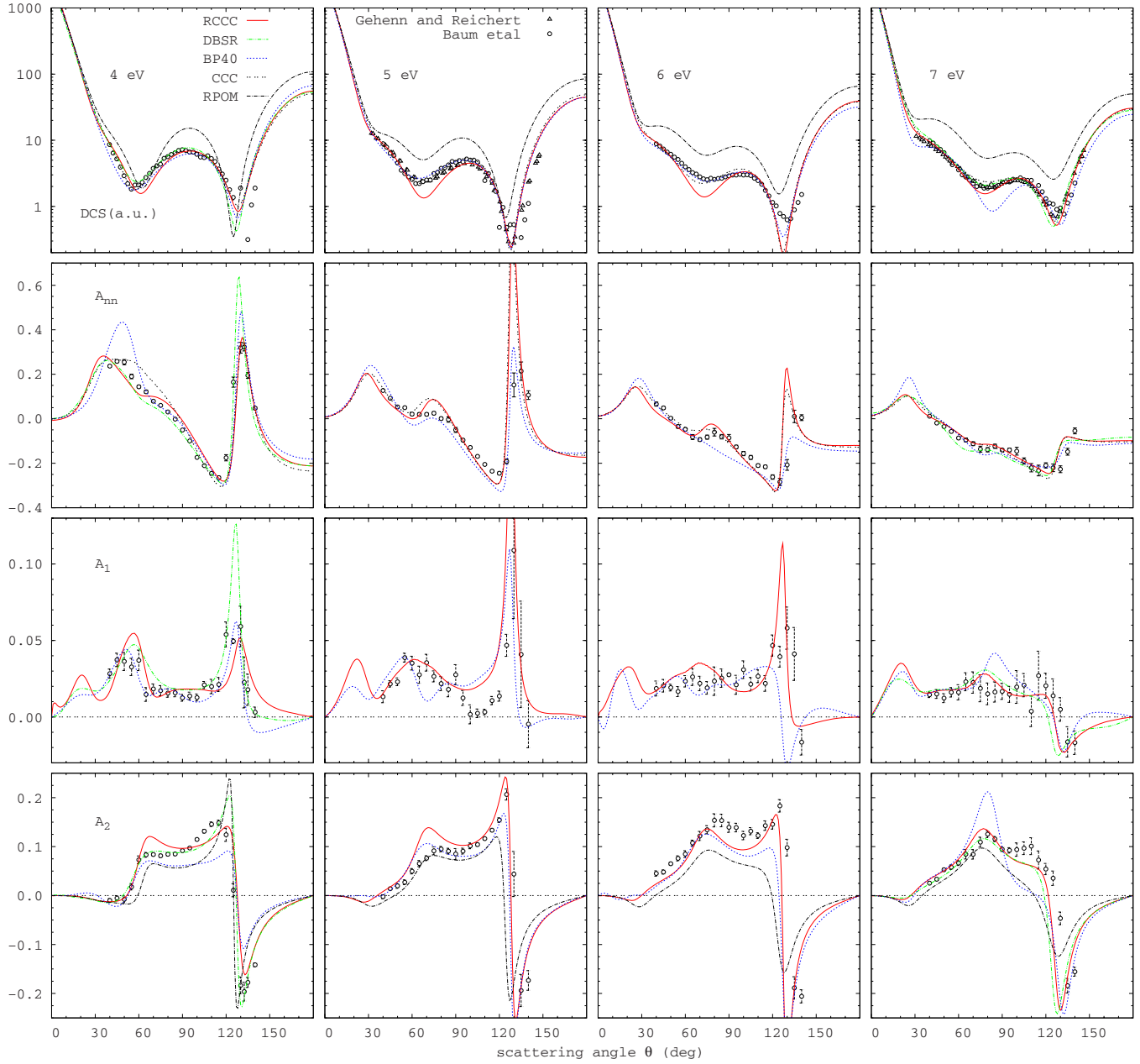

FIG. 3. (Color online) Differential cross sections and spin asymmetries for elastic electron scattering on the ground state of Cs at 4, 5, 6, and 7 eV incident electron energies. Present calculations (RCCC) are described in the text. Comparison is given with the results from the Dirac *R*-matrix (DBSR) calculations [16], 40-state semirelativistic Breit-Pauli *R*-matrix (BP40) calculations [7], nonrelativistic CCC calculations [7], and relativistic polarized-orbital method (RPOM) calculations [19]. Experiment is due to Gehenn and Reichert [43] and Baum *et al.* [7].

Calculation of the FBA-integrated cross sections,

$$\sigma_{fi}^{\mathrm{FBA}} = \int d\Omega \frac{d\sigma_{fi}^{\mathrm{FBA}}}{d\Omega}, \tag{71}$$

allows for an alternative implementation of the analytical Born subtraction technique for integrated cross sections that does not require evaluation of the scattering amplitude (64). This can be achieved by adopting the following expression for integrated cross sections:

$$\sigma_{fi} = \sum_{J\Pi} (\sigma_{fi}^{J\Pi} - \sigma_{fi}^{J\Pi,\mathrm{FBA}}) + \sigma_{fi}^{\mathrm{FBA}}, \tag{72}$$

where $\sigma_{fi}^{J\Pi,\mathrm{FBA}}$ is defined as in Eq. (54) but with $\tilde{V}_{fi}^{\Pi IJ}(k_f\kappa_f, k_i\kappa_i)$ matrix elements.

III. RESULTS

We have performed calculations of *e*-Cs scattering in the intermediate energy region from 4 to 25 eV using four models which differ in the number of states included in the close-

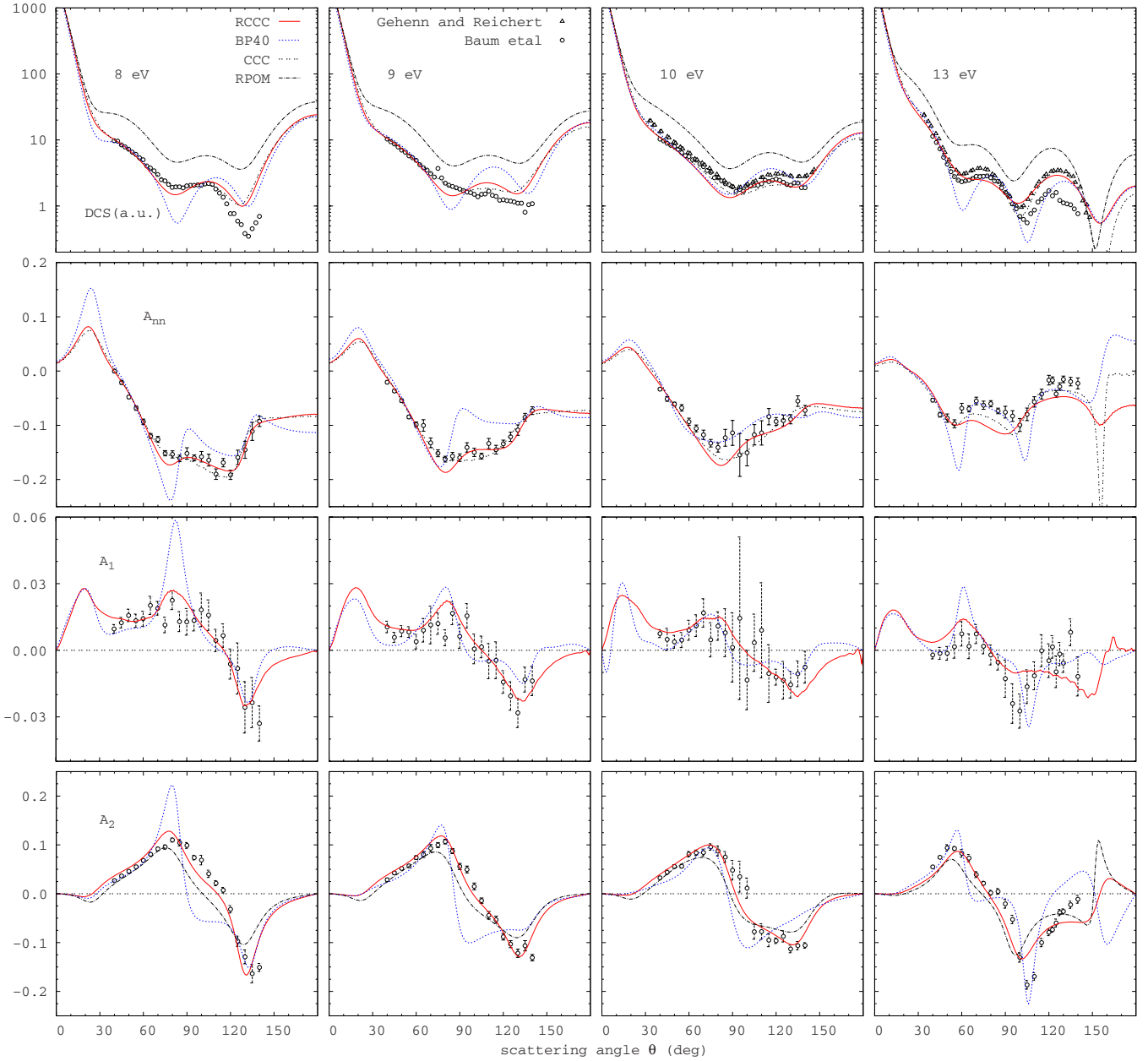

FIG. 4. (Color online) Same as in Fig. 3 but at 8, 9, 10, and 13 eV incident electron energies.

coupling expansion, namely, 12, 27, 75, and 89 states. The target states have been obtained by diagonalization of the cesium Hamiltonian in Dirac L spinor basis with exponential fall-off $\lambda=3.0$ and $N=75$ for each value of $\kappa=\pm1,\pm2,\pm3,4$. We have used the polarization potential obtained from the polarized-orbital method of McEachran *et al.* [23] and kept it the same for all target symmetries. The ionization energies of the lowest 12 states are presented in Table I and are found to be in good agreement with experimental values. More accurate treatment of the Cs target structure is possible via rescaling of the polarization potential to fit low-lying energy levels for each target symmetry. We will discuss the influence of the polarization potential on Cs atomic structure and e-Cs scattering calculations elsewhere.

The 12-state RCCC model includes the 12 lowest Cs bound states, the 27-state model includes all discrete spectrum states obtained from diagonalization, and the 75- and 89-state models include also a large number of pseudostates that allow us to model increasing coupling to the ionization continuum. Comparison between the results of these four models allows determining the convergence rate of the RCCC calculations. We have performed such a comparison at a number of energies with the 15 eV results presented in Fig. 2 being characteristic of other energies as well. Little difference between the RCCC(89) and RCCC(75) results demonstrates convergence for the parameters considered. Comparison between results from smaller models, eight-state and 27-state RCCCs, with the converged RCCC results shows that DCS and spin asymmetries A_1 and A_2 have a very

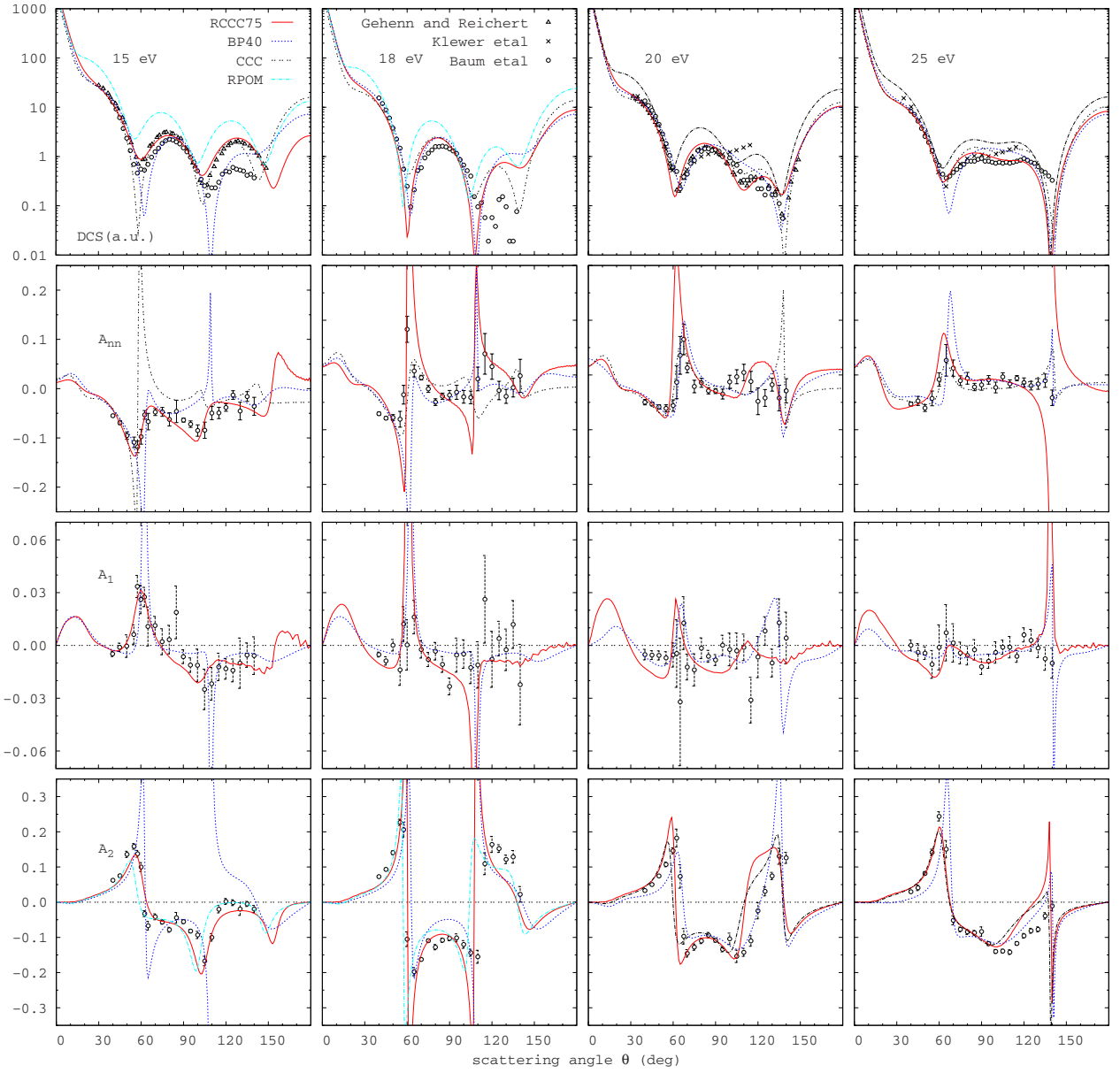

FIG. 5. (Color online) Same as in Fig. 3 but at 15, 18, 20, and 25 eV incident electron energies. In addition, an experiment due to Klewer *et al.* [44] is shown.

fast convergence rate as opposed to spin asymmetry A_{nn} which is strongly affected by channel coupling and requires inclusion of ionization channels to obtain a convergent result. We note also that a large partial-wave expansion (number of partial waves ≈60) combined with O'Malley-style extrapolation technique [42] to account for even higher partial waves is required to achieve smooth curves for asymmetries A_1 and A_2.

We present results of our RCCC 75-state calculations for elastic scattering in Fig. 3 for 4–7 eV, Fig. 4 for 8–13 eV, and Fig. 5 for 15–25 eV incident electron energies. Comparisons to previous calculations are presented for the nonrelativistic CCC method [7], relativistic polarized-orbital method (RPOM) [19], 40-state Breit-Pauli *R*-matrix method (BP40) [7], and at 4 and 7 eV with 30-state Dirac *B*-spline *R*-matrix (DBSR) method [16]. Experimental spin asymmetries and DCS are due to Baum *et al.* [7], as well as Gehenn and Reichert [43] and Klewer *et al.* [44] for DCS only. We have normalized both sets of (relative) DCS data to achieve the best visual fit to the RCCC(75) DCS.

Good agreement with experimental DCS is found across all considered energies. At some energies, 13 and 15 eV, our results seem to favor the shape of the DCS of Gehenn and Reichert [43]. At a number of other energies, from 4 to 10 eV, the shape of the RCCC(75) DCS is somewhat different to the measured data [7] at intermediate scattering angles where the DCSs are particularly small. We find that in this region, the DCS are strongly influenced by the choice of the polarization potential. For example, the choice of a simple model

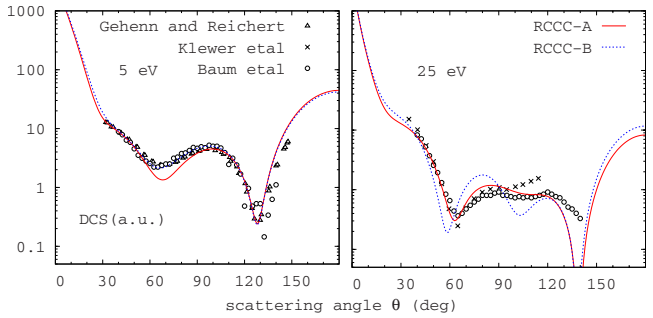

FIG. 6. (Color online) Differential cross sections for elastic electron scattering on the ground state of Cs at 5 and 25 eV incident electron energies. Comparison of the results from the RCCC75 calculations conducted with *ab initio* polarization potential of [23] (RCCC-A) and model polarization potential [4] (RCCC-B). Experiment is due to Gehenn and Reichert [43], Klewer *et al.* [44], and Baum *et al.* [7].

polarization potential [4] which has been adopted in our previous publication [1] leads to a little better DCS shapes at low energies, but slightly worse shapes at 13 eV and larger energies. This is illustrated in Fig. 6 at the two energies of 5 and 25 eV. We will discuss this issue in more detail elsewhere. Comparing to other calculations of the DCS, we find generally good agreement between all the close-coupling calculations regardless of whether they have been performed in a fully relativistic formulation (RCCC, DBSR), a semirelativistic Breit-Pauli approach (BP40), or in a nonrelativistic method (CCC). Occasional differences between close-coupling theoretical results are likely to be due to the differences in the atomic structure details. On the other hand, the RPOM results of Ahmed *et al.* [19] are in substantial disagreement with our and other close-coupling calculations for all considered energies. Given that RPOM is a first-order method, its region of validity is the high energies. Therefore, it is perhaps not surprising to see such discrepancies at the considered energies. Accurate account of channel coupling effects, which are neglected or severely approximated in first-order methods, is apparently important to obtain correct DCS shapes and absolute values even at 25 eV, which is a relatively higher energy (4 times the ionization threshold) for *e*-Cs scattering.

It is interesting to note that the region below 10 eV, where our calculations exhibit some differences with the experimental DCS, is also where we have very good agreement with the experimental spin asymmetries [7]. Similarly good agreement is found at energies above 10 eV. The spin asymmetries are ratio parameters. Hence, they are free from uncertainties associated with DCS normalization and have proved to be a very reliable set of experimental data. The asymmetry A_{nn}, also known as the exchange asymmetry, is strongly influenced by the projectile-target electron exchange and is the only asymmetry parameter that is nonzero when calculated in nonrelativistic methods. The nonrelativistic CCC method proved to be very successful in predicting accurate exchange asymmetry A_{nn}. The BP40 results are generally in good agreement with experiment at most of the considered energies. Our investigation indicates that treatment of the exchange with the Cs core electrons in a local exchange approximation in the BP40 model and the choice of polarization potential are responsible for most of the differences. The DBSR method results presented at 4 and 7 eV in Fig. 3 are generally in very good agreement with our results. We note that for A_2 at 4 eV, the DBSR results are in better agreement with experiment. The DBSR method differs from RCCC and other methods in its treatment of interaction with the Cs core electrons. It is likely that at low incident electron energies, the full treatment of core-valence correlations adopted in the DBSR method becomes important. The results from RPOM calculations of Ahmed *et al.* [19], available for the A_2 asymmetry parameter only, are in a reasonably good agreement with experiment across all energies, which is somewhat unexpected given the rather poor agreement for the DCS. We also note very close agreement between RPOM and RCCC results, especially for larger energies. Both methods share practically the same Cs structure model of one active electron above a frozen Dirac-Fock core with the addition of the same polarization potential. Good agreement between RPOM and RCCC indicates that the correct account of relativistic effects and the Cs atomic structure seems to play a more important role than an accurate account of interchannel coupling. The insensitivity of the A_2 asymmetry parameter to channel coupling effects can also be seen in Fig. 2.

IV. CONCLUSION

In this paper, we have presented a detailed formulation of the RCCC method and verified it against a comprehensive set of DCS and spin asymmetry measurements for *e*-Cs elastic scattering. Treatment of the relativistic effects in the RCCC method is carried out fully *ab initio* via solution of the Dirac equation. The important advantage of the nonrelativistic CCC method, its ability to produce accurate results across all energy ranges, is retained in the relativistic formulation as well. This is achieved by using the relativistic equivalent of the Sturmian (Laguerre) representation of the target Hamiltonian [25].

Application of the RCCC method to *e*-Cs elastic scattering demonstrated the high accuracy of the RCCC method and in a number of cases provided significant improvement over previous theoretical results. It has also revealed a number of problems that require further investigation. We find that modeling core-valance electron-electron interaction via a frozen-core model generally produces good results although the choice of the core-polarization potential becomes an important issue for a target as heavy as cesium.

The presented formalism allows for a straightforward extension to scattering problems involving highly charged ions via the inclusion of relativistic correction terms to the Coulomb electron-electron interaction potential [45]. Extension of the RCCC method to electron scattering from quasi-two-electron atoms is underway.

ACKNOWLEDGMENTS

The authors would like to thank Dr. Quiney for helpful discussions and Professor Bartschat, Professor Stauffer, and

Dr. Zatsarinny for sending their data in electronic form. We are grateful to Professor McEachran for sending us numerical values of the polarization potential. This work was supported by the Australian Research Council. We are grateful for the access to the Australian National Computational Infrastructure and its Western Australian node iVEC.

[1] D. V. Fursa and I. Bray, Phys. Rev. Lett. **100**, 113201 (2008).
[2] M. Maslov, M. J. Brunger, P. J. O. Teubner, O. Zatsarinny, K. Bartschat, D. Fursa, I. Bray, and R. P. McEachran, Phys. Rev. A **77**, 062711 (2008).
[3] I. Bray and A. T. Stelbovics, Phys. Rev. Lett. **69**, 53 (1992).
[4] I. Bray, Phys. Rev. A **49**, 1066 (1994).
[5] D. V. Fursa and I. Bray, Phys. Rev. A **52**, 1279 (1995).
[6] D. V. Fursa and I. Bray, J. Phys. B **30**, 5895 (1997).
[7] G. Baum, N. Pavlovic, B. Roth, K. Bartschat, Y. Fang, and I. Bray, Phys. Rev. A **66**, 022705 (2002).
[8] G. Baum, S. Förster, N. Pavlovic, B. Roth, K. Bartschat, and I. Bray, Phys. Rev. A **70**, 012707 (2004).
[9] D. S. Slaughter, V. Karaganov, M. J. Brunger, P. J. O. Teubner, I. Bray, and K. Bartschat, Phys. Rev. A **75**, 062717 (2007).
[10] D. V. Fursa and I. Bray, Phys. Rev. A **59**, 282 (1999).
[11] D. V. Fursa, I. Bray, and G. Lister, J. Phys. B **36**, 4255 (2003).
[12] J.-J. Chang, J. Phys. B **8**, 2327 (1975).
[13] P. H. Norrington and I. P. Grant, J. Phys. B **14**, L261 (1981).
[14] S. Ait-Tahar, I. P. Grant, and P. H. Norrington, Phys. Rev. Lett. **79**, 2955 (1997).
[15] M. J. Vilkas and Y. Ishikawa, Phys. Rev. A **75**, 062508 (2007).
[16] O. Zatsarinny and K. Bartschat, Phys. Rev. A **77**, 062701 (2008).
[17] O. Zatsarinny and K. Bartschat, Phys. Rev. A **79**, 042713 (2009).
[18] N. R. Badnell, J. Phys. B **41**, 175202 (2008).
[19] M. F. Ahmed, W. Ji, R. P. McEachran, and A. D. Stauffer, J. Phys. B **40**, 4119 (2007).
[20] V. Zeman, R. P. McEachran, and A. D. Stauffer, J. Phys. B **27**, 3175 (1994).
[21] K. G. Dyall, I. P. Grant, C. T. Johnson, F. P. Parpia, and E. P. Plummer, Comput. Phys. Commun. **55**, 425 (1989).
[22] P. Strange, *Relativistic Quantum Mechanics* (Cambridge University Press, London, 1998).
[23] R. P. McEachran, D. L. Morgan, A. G. Ryman, and A. D. Stauffer, J. Phys. B **10**, 663 (1977).
[24] W. Kutzelnigg, Int. J. Quantum Chem. **25**, 107 (1984).
[25] I. P. Grant and H. M. Quiney, Phys. Rev. A **62**, 022508 (2000).
[26] R. Szmytkowski, J. Phys. B **30**, 825 (1997).
[27] I. S. Gradshteyn and I. M. Ryzhik, *Tables of Integrals, Series and Products* (Academic Press, San Diego, 1980).
[28] P. A. M. Dirac, Proc. R. Soc. London, Ser. A **118**, 351 (1928).
[29] I. P. Grant, Adv. Phys. **19**, 747 (1970).
[30] I. Bray and A. T. Stelbovics, Phys. Rev. A **46**, 6995 (1992).
[31] R. H. Landau, *Quantum Theory II: Second Course in Quantum Theory* (Wiley Interscience, New York, 1989).
[32] A. T. Stelbovics, Phys. Rev. A **41**, 2536 (1990).
[33] J. Sucher, Phys. Rev. A **22**, 348 (1980).
[34] I. P. Grant, *Relativistic Quantum Theory of Atoms and Molecules: Theory and Computations* (Springer, New York, 2007).
[35] M. Rose, *Relativistic Electron Theory* (John Wiley and Sons, New York, 1961).
[36] J. E. Sienkiewicz and W. E. Baylis, J. Phys. B **20**, 5145 (1987).
[37] F. Salvat, J. M. Fernandez-Varea, and W. Williamson, Jr., Comput. Phys. Commun. **90**, 151 (1995).
[38] C. J. Joachain, *Quantum Collision Theory*, 3rd ed. (Elsevier Science Publishers B. V., Amsterdam, 1983).
[39] K. Bartschat and Y. Fang, Phys. Rev. A **62**, 052719 (2000).
[40] M. Inokuti, Rev. Mod. Phys. **43**, 297 (1971).
[41] C. J. Fontes and H. L. Zhang, Phys. Rev. A **76**, 040703(R) (2007).
[42] L. J. Allen, I. Bray, and I. E. McCarthy, Phys. Rev. A **37**, 49 (1988).
[43] W. Gehenn and E. Reichert, J. Phys. B **10**, 3105 (1977).
[44] M. Klewer, M. J. M. Beerlage, and M. J. V. der Weil, J. Phys. B **12**, L525 (1979).
[45] C. J. Bostock, D. V. Fursa, and I. Bray (unpublished).
[46] C. E. Moore, *Atomic Energy Levels*, Natl. Bur. Stand. (U.S.) Circ. No. 467 (U.S. GPO, Washington, D.C., 1949), Vol. III.